

Auxin Stimulates Its Own Transport by Shaping Actin Filaments¹

Peter Nick*, Min-Jung Han, and Gyeunhung An

Institute of Botany 1, University of Karlsruhe, D-76128 Karlsruhe, Germany (P.N.); and National Research Laboratory of Plant Functional Genomics, Department of Life Science, Pohang University of Science and Technology (POSTECH), Pohang 790-784, Republic of Korea (M.-J.H., G.A.)

The directional transport of the plant hormone auxin has been identified as central element of axis formation and patterning in plants. This directionality of transport depends on gradients, across the cell, of auxin-efflux carriers that continuously cycle between plasma membrane and intracellular compartments. This cycling has been proposed to depend on actin filaments. However, the role of actin for the polarity of auxin transport has been disputed. The organization of actin, in turn, has been shown to be under control of auxin. By overexpression of the actin-binding protein talin, we have generated transgenic rice (*Oryza sativa*) lines, where actin filaments are bundled to variable extent and, in consequence, display a reduced dynamics. We show that this bundling of actin filaments correlates with impaired gravitropism and reduced longitudinal transport of auxin. We can restore a normal actin configuration by addition of exogenous auxins and restore gravitropism as well as polar auxin transport. This rescue is mediated by indole-3-acetic acid and 1-naphthyl acetic acid but not by 2,4-dichlorophenoxyacetic acid. We interpret these findings in the context of a self-referring regulatory circuit between polar auxin transport and actin organization. This circuit might contribute to the self-amplification of auxin transport that is a central element in current models of auxin-dependent patterning.

In addition to its role as central regulator of growth, auxin is involved in pattern formation (Berleth and Sachs, 2001). Auxin-dependent patterning is linked to a directional flow of auxin, a cell-to-cell transport described by a modified chemiosmotic model (Lomax et al., 1995). The self-amplification of cell polarity by a polar auxin flow has been linked with directional intracellular traffic. Positive feedback of auxin on this traffic in combination with mutual competition of neighboring cells for free auxin are central for pattern formation (Merks et al., 2007). This so-called auxin canalization model has been originally deduced from an analysis of vascular bundles in regenerating stems (Sachs, 1969) but was successfully applied to venation in developing leaves (Sachs, 2000) and the patterning of leaf primordia (Reinhard et al., 2000). Thus, patterning would ultimately depend on the directionality of auxin transport.

In the meantime, several plant-specific pin-formed (PIN) proteins have been identified as candidates for

auxin-efflux carriers (for review, see Chen and Masson, 2006), and despite a long debate on the actual function of these proteins, the most recent results show that they are in fact rate-limiting for auxin efflux (Petrášek et al., 2006). PIN proteins undergo constitutive recycling between plasma membranes and endosomal compartments (Geldner et al., 2001; Paciorek et al., 2005). This recycling seems to be under control of small GTPases, the ADP-ribosylation factors (ARFs), and their associated guanine nucleotide exchange factors (Geldner et al., 2003). Mutation of one of these guanine nucleotide exchange factors is responsible for the phenotype of the Arabidopsis (*Arabidopsis thaliana*) mutant *gnom* causing a mislocalization of PIN1 that becomes trapped in intracellular compartments. This cellular mutant phenotype can be phenocopied by treatment of the wild type with brefeldin A, a fungal toxin that selectively blocks ARF-guanine nucleotide exchange factors (Geldner et al., 2001). This suggests that ARF-dependent vesicle trafficking is involved in the polar distribution of PIN proteins and, thus, in cell polarity.

The internalization of PIN1 caused by brefeldin A is arrested by the actin inhibitor cytochalasin D (Geldner et al., 2001). Conversely, PIN3 is rapidly internalized upon treatment with cytochalasin (Friml et al., 2002). Moreover, the potent actin inhibitor latrunculin B (LatB) impaired the polar localization of PIN1 in protophloem cells, and with even higher sensitivity, of the auxin-efflux carrier AUX1 (Kleine-Vehn et al., 2006), and inhibition of myosin function with butane-

¹ This work was in part supported by a grant from the Biogreen 21 program, Rural Development Administration (to G.A.), and the German Research Council (Priority Programme Phytohormones; P.N.).

* Corresponding author; e-mail peter.nick@bio.uni-karlsruhe.de.

The author responsible for distribution of materials integral to the findings presented in this article in accordance with the policy described in the Instructions for Authors (www.plantphysiol.org) is: Peter Nick (peter.nick@bio.uni-karlsruhe.de).

www.plantphysiol.org/cgi/doi/10.1104/pp.109.140111

2,3 monoxime inhibited basipetal auxin transport in flower stalks of *Arabidopsis* (Holweg, 2007). These findings suggest that actin participates in the cycling of some of the PIN proteins.

The relation between actin and auxin seems to be bidirectional but complex; as early as 1937, Sweeney and Thimann (1937) demonstrated that auxin stimulates cytoplasmic streaming in oat (*Avena sativa*) coleoptiles. However, when streaming was inhibited by cytochalasin B, this delayed the onset of auxin transport but left the rate of auxin transport unaltered (Cande et al., 1973). The stimulation of coleoptile growth by auxin is accompanied by a debundling of actin bundles into finer strands (Waller et al., 2002; Holweg et al., 2004).

Inhibition of auxin transport impaired the organization of actin in zygotes of the brown alga *Fucus* and inhibited signal-induced developmental polarity (Sun et al., 2004). Since the cycling of PIN proteins is regulated by auxin itself (Paciorek et al., 2005), there might be a feedback loop between actin and auxin. Consistent with this view, binding sites for 1-*N*-naphthylphthalamic acid (NPA), an inhibitor of polar auxin transport, have been found to cosediment with actin (Butler et al., 1998).

However, models that link the polar localization of the PIN proteins to actin-dependent transport (Muday and Murphy, 2002; Blakeslee et al., 2005) are challenged by experiments where PIN proteins maintained their polar localization, although actin filaments had been eliminated (for instance, by cytochalasin D [Geldner et al., 2001], by low concentrations of LatB [Kleine-Vehn et al., 2006], or by the phytohormone NPA or artificial auxin 2,4-dichlorophenoxyacetic acid [2,4-D; Rahman et al., 2007]).

On the other hand, a recent report (Dhonukshe et al., 2008) demonstrated that 2,3,5-triiodobenzoic acid (TIBA) and the phytohormone 2-(1-pyrenoyl) benzoic acid induced actin bundling not only in plants, but also in mammalian and yeast cells, i.e. in cells that are not to be expected to use auxin as signaling compound. This was interpreted as supportive evidence for a role of actin filaments in polar auxin transport. However, it was mentioned in the same work that NPA failed to cause actin bundling in nonplant cells, suggesting that its mode of action must be different. This is consistent with classical work demonstrating that different phytohormones act on different targets (for review, see Rubery, 1990). Summarizing, although actin seems to play a role for the polarity of auxin fluxes, this issue is, first, not simple and, second, far from being understood.

The relationship between actin and auxin was studied in the context of patterned cell division using the tobacco (*Nicotiana tabacum*) cell line BY-2 (Maisch and Nick, 2007). In this cell line, cell division is partially synchronized within a cell file, leading to higher frequencies of files with even cell numbers compared with files with uneven cell numbers. This synchrony can be interrupted by low concentrations of NPA, an

inhibitor of polar auxin flux. To address the role of actin in this synchrony, the actin-binding protein mouse talin was overexpressed in those cells, resulting in a bundled configuration of actin and a loss of synchrony similar to the effect of NPA (indicative for a reduced auxin transport). By addition of auxins that are transported in a polar fashion (but not auxin per se), both the normal organization of actin (with fine strands) and the synchrony of cell division could be restored. This demonstrated that debundled actin strands are necessary and sufficient for the synchrony of cell division. However, although being indicative for a functional auxin transport, this synchrony is not a direct measure of auxin transport.

To measure auxin transport directly, it would be necessary to administer radioactively labeled auxin to one pole of the file and to quantify the radioactivity recovered in the opposite pole of the file. This is not possible in a tobacco cell culture that has to be cultivated as suspension in a liquid medium. We therefore have returned to the classical Graminean coleoptile system (for a classical review, see Goldsmith, 1977), where auxin has been discovered originally by its polar transport and where auxin transport can be easily measured by following the distribution of radioactively labeled indole-3-acetic acid (IAA) fed to the coleoptile apex. We generated transgenic rice (*Oryza sativa*) lines expressing the actin-binding protein talin to variable levels. In those lines, as a consequence of talin overexpression, actin filaments were bundled to variable extent. The bundling of actin filaments was accompanied by a reduced polar transport of auxin. We could restore a debundled configuration of actin by addition of exogenous auxin, and by this treatment we were able to restore auxin transport. This rescue was mediated by transportable auxin species, but not by the artificial auxin 2,4-D that lacks polar transport. Using this approach, we can now probe the causal relationship between actin configuration and polar auxin transport directly.

RESULTS

Yellow Fluorescent Protein-Mouse Talin Bundles Actin Depending on Expression Level

Seedlings transgenic for 35S::yellow fluorescent protein-mouse talin (YFP-mT) developed normally and did not display obvious morphological differences as long as the expression level was moderate (such as the line L5, Fig. 1H). Even for strong expression (such as in the line L6, Fig. 1H), there were only minor alterations of development, such as slightly reduced plagiotropism in leaf sheaths or a subtle reduction of flag leaves upon flower induction. Fluorescent filaments could be observed in all tissues of these seedlings that were found to consist of F-actin upon staining with fluorescent phalloidin (Fig. 1A). In Graminean seedlings, actin is specifically reorganized during development

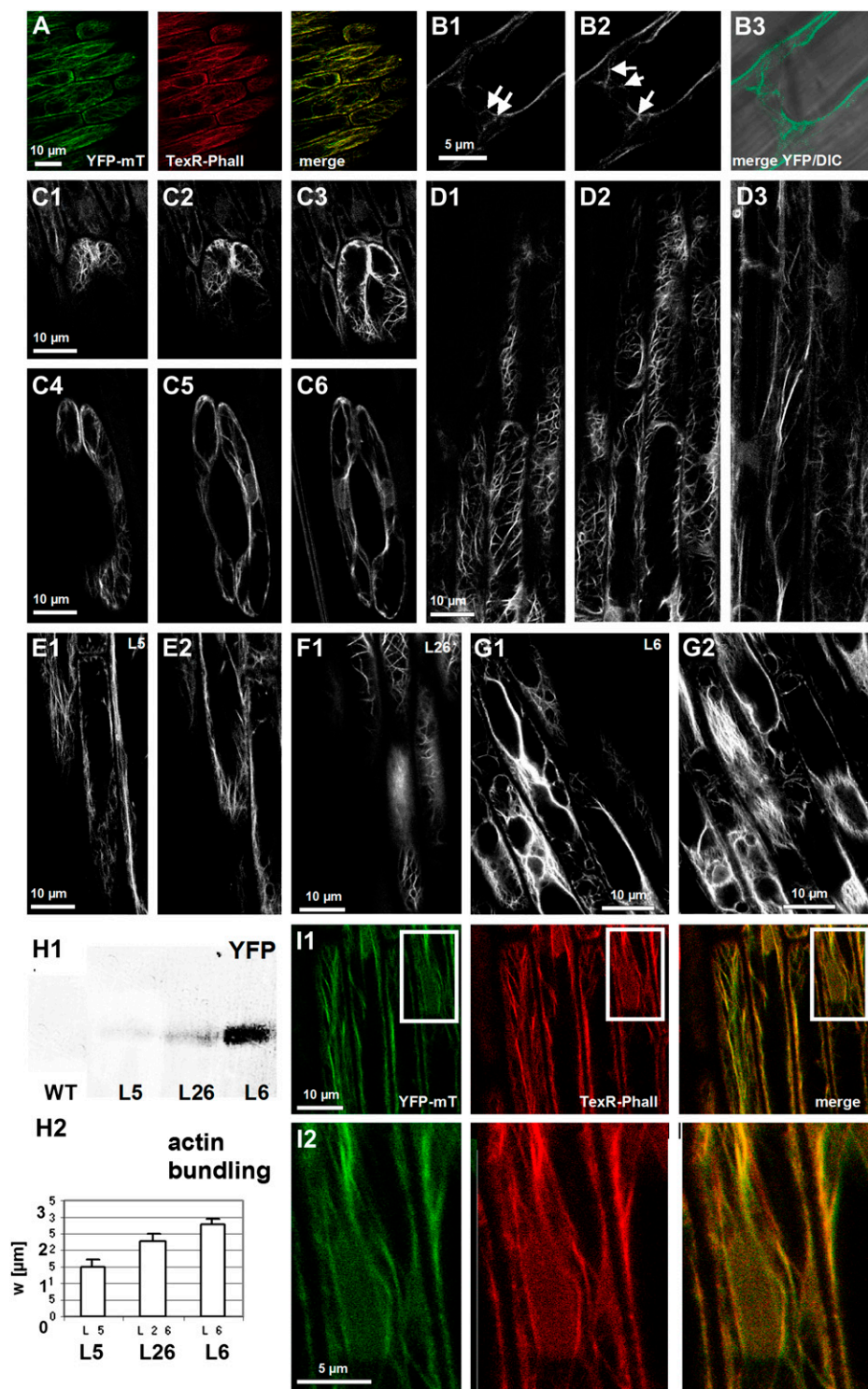


Figure 1. Visualization of actin filaments in rice seedlings through stable expression of YFP-mT. A, Dual visualization of actin filaments through YFP-mT (green) versus conventional staining with TexasRed-conjugated phalloidin (TexR-Phall; red) in the moderate expressor line L5. The merge of the two channels (yellow) shows high congruence for the two modes of visualization. B, Polar meshwork of actin filaments extending through cross-walls (white arrows), confocal sections of a fully expanded coleoptile epidermal cell (B1 and B2), and merge of YFP and differential interference contrast (DIC) image (B3). C, Reorganization of actin filaments during elongation of guard cells and confocal sections of a guard cell recorded at day 4 after germination (C1–C3) and after full expansion of the coleoptile at day 6 after germination (C4–C6). D, Tissue-specific organization of actin filaments in the primary roots, confocal sections of epidermis (D1 and D2), and cortex (D3). The images in A to D were recorded in the moderate expressor line L5. E to H, Dependence of actin organization on the level of expression of YFP-talin. Confocal sections of epidermal cells in fully expanded coleoptiles of transgenic lines L5 (moderate expression; E1 and E2), L26 (high expression; F1), and L6 (very high expression; G1 and G2). The expression of YFP-mT was probed by western blotting of total coleoptile extracts using a polyclonal anti-FP antibody (H1), and the apparent mean width of actin strands (w; see Fig. 4C) was assessed as measure for the degree of actin bundling (H2). WT, Wild type. I, Dual visualization of actin filaments through YFP-mT (green) and TexasRed-conjugated phalloidin (red) in the high-expression line L6 to test whether the diffuse YFP signal is produced by F-actin. The global view is shown in I1; the inset is zoomed in I2 to show the congruence between the diffuse YFP signal with the TexasRed signal.

and dependently on the respective tissue (Waller and Nick, 1997). This reorganization is reliably recorded by the YFP-mT marker. For instance, we could observe the characteristic polar meshwork of actin (Fig. 1B) that in seedlings of the *Poaceae* reaches through the cross-walls of adjacent epidermal cells via the plasmodesmata (Waller et al., 2002), or we could follow the

reorientation of actin in guard cells during coleoptile expansion (Fig. 1C), and we could see the tissue-specific actin arrays in the primary root (Fig. 1D). Thus, in these lines, the tissue-dependent and developmental reorganization of actin was faithfully mirrored by the YFP-mT marker without detectable aberrations of actin organization. However, this was

not true for lines where YFP-mT was expressed to higher levels (such as the lines L26 and L6, Fig. 1H1). In these strong expressors, actin filaments were bundled, and diffuse actin was present in the cortical cytoplasm (Fig. 1, F, G, and H2). To test, whether this diffuse signal was caused by dissociation of excess YFP-mT marker from actin, we performed a double visualization with TexasRed-conjugated phalloidin (Figs. 1I1 and 2) in the strong expressor line L6 and observed that the diffuse YFP signal was completely congruent with the TexasRed signal, indicating that this diffuse signal is caused by F-actin. In conclusion, YFP-mT can be used as marker to follow actin organization in vivo as long as the abundance of this marker is moderate. Upon strong expression, YFP-mT produces actin bundles. We therefore focused our analysis on line L5 as representative of the moderate expressors and line L6 as representative of the strong expressor lines.

YFP-mT Affects Actin Dynamics Depending on Expression Level

To assess the dynamics of actin filaments, we followed dislocations of actin filaments over time. Whereas the filaments changed dynamically in the moderate expressor line L5 (Fig. 2A), they were very static in the strong expressor line L6 (Fig. 2B). Although in L6 bundles were thicker on average compared to L5, there is a distribution of thickness in both lines, and there is overlap, i.e. there are bundles in L6 that can be thinner than thicker bundles in L5. Moreover, actin filaments occur in different configurations, with transvacuolar bundles generally being thicker than cortical strands. However, even for bundles of comparable thickness, the dynamicity of actin filaments was lower in L6 compared to L5 (compare Fig. 2, A and B). To quantify this qualitative result, we recorded time series and generated the absolute dif-

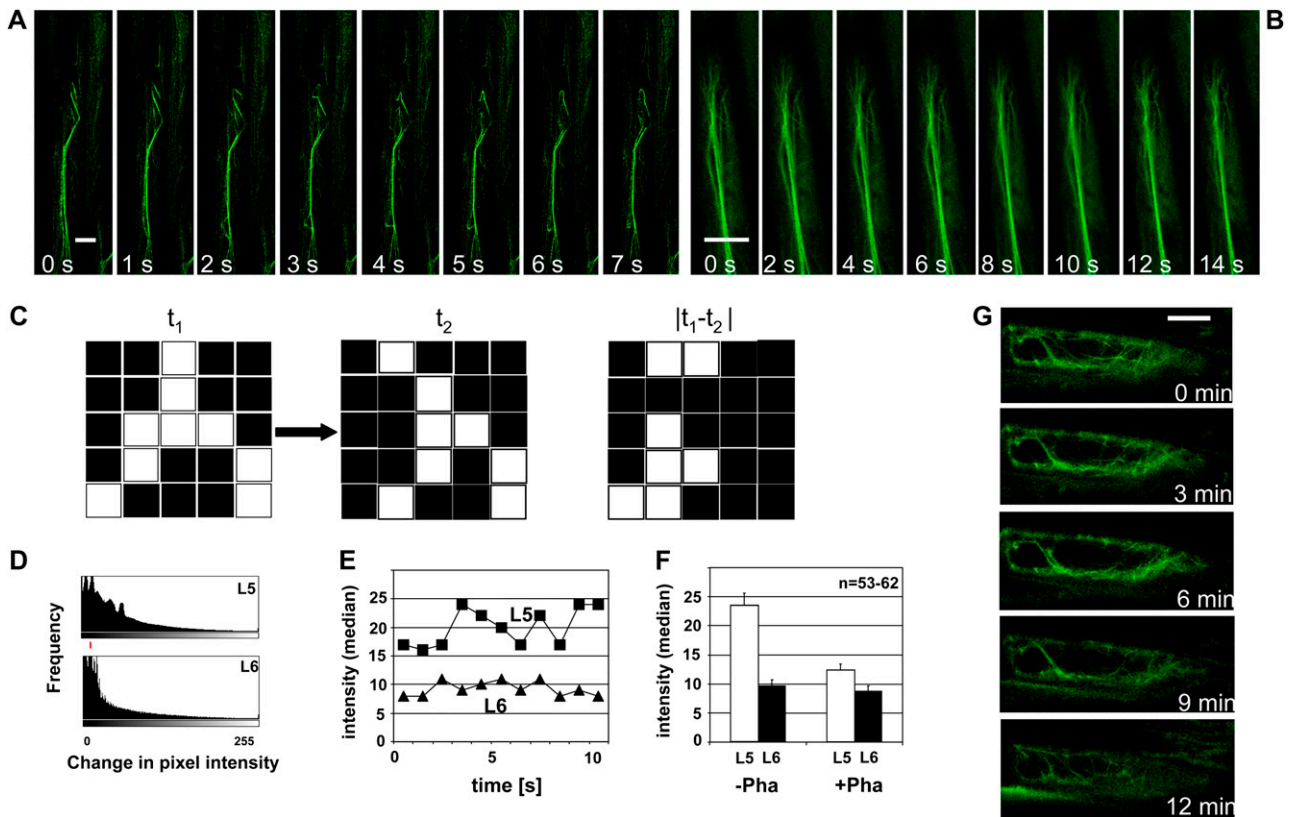


Figure 2. Dynamics of actin filaments in epidermal cells expressing moderate (A) or very high (B) levels of YFP-mT. A and B, Time-lapse series of individual filaments in L5 (moderate expression; A) or L6 (very high expression; B). Bundles of comparable thickness are shown. Bars = 2.5 μm . C, Illustration of the method used to quantify actin dynamics. Two subsequent frames of a time-lapse series (t_1 and t_2) are subtracted to yield the differential $|t_1 - t_2|$. The pixel intensities of this differential increase proportional to the shifts of the filaments between t_1 and t_2 . D, Typical histogram over the change in pixel intensity between subsequent snapshots of a time-lapse series recorded in L5 and L6 as indicator for actin dynamics. The red line shows the respective median values. E, Average shifts of pixel intensity (median values of histograms as shown in D) over time in individual cells of lines L5 and L6, respectively. F, Average values of histogram averages (as shown in E) over populations of epidermal cells from L5 (moderate expression; white bars) or L6 (very high expression; black bars) in control plants (-Pha) or after treatment with 1 μM phalloidin for 1 h (+Pha), respectively. Between 53 and 62 individual cells were scored for each line. G, Response of actin filaments to treatment with 10 μM LatB in L5.

differentials between images of subsequent time points (Fig. 2C). For static filaments, this operation would result in low pixel intensities, and for filaments that had shifted position during the time interval between two frames, high pixel intensities would result. In L5, the frequency histograms over the pixel intensities of these differentials were much broader, and the distribution medians were persistently higher (Fig. 2, D and E) compared to L6. On average, the dynamics of actin filaments in L6 was reduced by >50% compared to L5 (Fig. 2F, -Pha). By treatment with 1 μM of the actin-bundling drug phalloidin, actin dynamics in L5 could be decreased to about 50%, whereas there was almost no response in L6 (Fig. 2F, +Pha). We further tested whether the filaments are sensitive to latrunculins. This class of inhibitors irreversibly sequesters G-actin such that actin filaments are eliminated depending on their innate turnover (Coué et al., 1987). Upon treatment with 10 μM LatB, actin filaments in L5 could be efficiently eliminated within 12 min, indicating rapid turnover of G-actin (Fig. 2G).

YFP-mT Affects Gravitropism Depending on Expression Level

To test for the physiological consequences of the reduced actin dynamics in line L6, we chose coleoptile gravitropism as test response because it is driven by polar auxin transport (Gutjahr and Nick, 2006) and depends on actin dynamics (Wang and Nick, 1998). The amplitude of gravitropism in 38 independent lines plotted over the expression of the YFP-mT protein (relative to the strongest expressor L6) revealed that curvature was not significantly different from the nontransformed wild type as long as the relative abundance of the YFP-mT protein did not exceed 0.5 (Fig. 3A). However, for stronger expression, the gravitropic response became inhibited by >50% compared to the wild-type value. Thus, actin bundling upon strong overexpression of YFP-mT was accompanied by an inhibition of gravitropism. To understand this effect in more detail, we recorded dose-response curves for the inhibition of auxin-induced growth (Fig. 3B) and gravitropic curvature (Fig. 3, D and E) over LatB. The dose response of the elongation of coleoptile segments to exogenous IAA (Fig. 3C) was bell-shaped with a peak at around 5 μM of IAA. However, the amplitude of this curve was reduced in the strong expressor L6 to about half of the growth increment observed in the wild type and the moderate expressor L5. Both cell elongation and gravitropism were inhibited in the wild type and the moderate expressor L5 as soon as the concentration of latrunculin exceeded 1 μM (Fig. 3, B and D). In contrast, they persisted up to 100 μM in L6 before a significant inhibition became detectable. This resistance is observed on the background of a generally reduced response amplitude in the strong expressor line L6, relative to the response in the absence of LatB (Fig. 3E), and the resistance of L6 was even more evident. To test whether the lines differed in

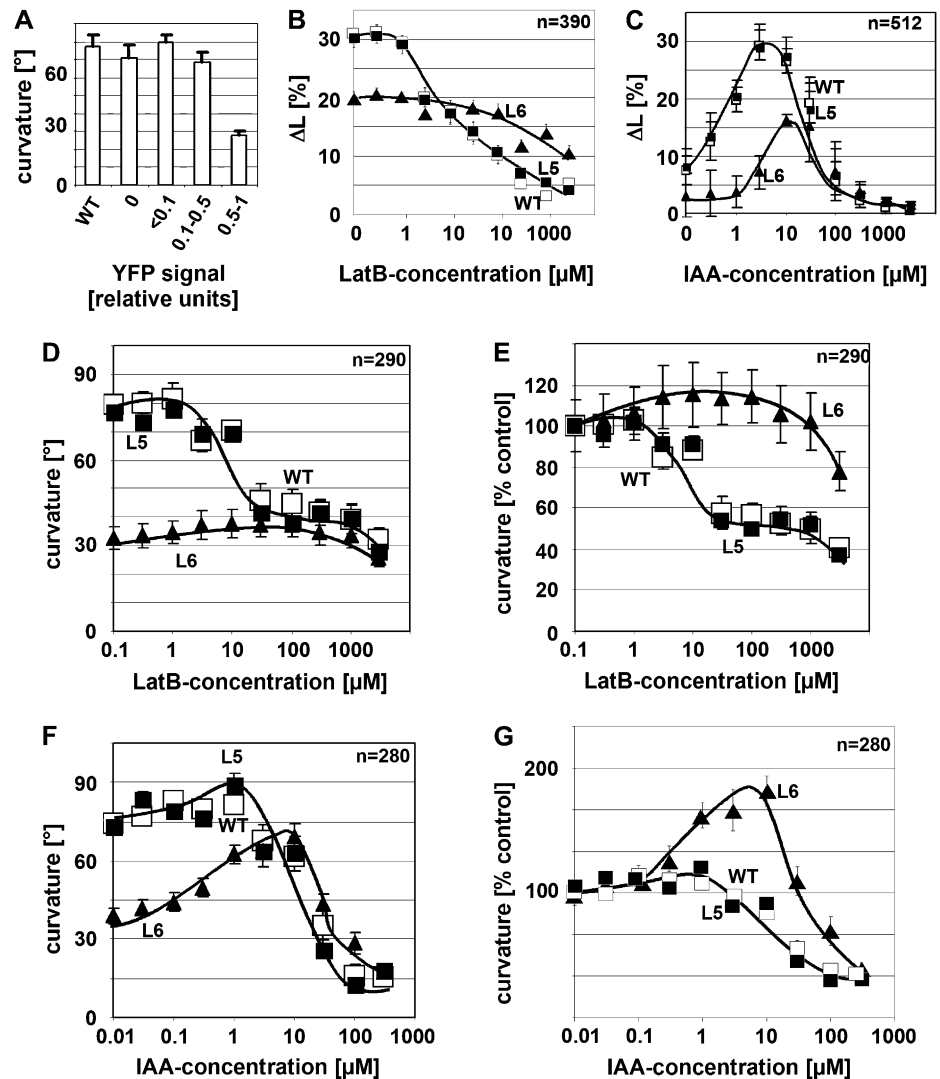
their response to auxin, we recorded the dose-response relations for gravitropism over exogenous auxin (using IAA). In the wild type and L5, curvature was slightly enhanced by auxin concentrations up to 1 μM but became progressively inhibited when the concentration of auxin was raised further (Fig. 3, F and G). For L6, the stimulation was more pronounced, and the peak was shifted to higher concentrations by about one order of magnitude. In summary, the physiological characteristics for moderate expression of YFP-mT (line L5) were found to be indistinguishable from the nontransformed wild type. In contrast, strong expression (line L6) resulted in a reduced gravitropic curvature and a reduced growth increment accompanied by a reduced sensitivity to both LatB and exogenous auxin.

These physiological effects were observed under inductive conditions. We have also followed the phenotype of the overexpressors through development but found that long-term behavior of seedlings and plants was fairly normal, even in L6. There was a tendency toward reduced plagiotropism in leaf sheaths and a slight reduction of flag leaves upon flower induction in L6 (data not shown). However, both effects were not statistically significant, at least not under greenhouse conditions. As already seen in Figure 3, the gravitropic responses of L6 were delayed, but for ongoing stimulation, it did reach the vertical. Thus, the long-term development in this line was not affected in the same manner as the inductive responses.

Auxin Rescues Actin Organization in a YFP-Talin Overexpressor

Actin bundling is controlled by auxins (Waller et al., 2002; Maisch and Nick, 2007). We therefore tested whether exogenous IAA can rescue the overexpression phenotype of L6 and followed the actin response to auxin in epidermal cells of dark-grown coleoptiles (Fig. 4A). We observed that auxin induced a transformation of massive longitudinal bundles into finer strands, detectable from around 10 to 20 min and completed within 30 to 60 min after addition of IAA, depending on the concentration of IAA. Conversely, when coleoptiles were decapitated in the moderate expressor line L5 to deplete the tissue from endogenous auxin, actin filaments became bundled within 30 min (Fig. 4B). To quantify these responses, we measured the average density of actin filaments as well as the average thickness of the bundles, as depicted in Figure 4C. For the moderate expressor lines L5 and L26 as well as for the strong expressor line L6, auxin induced an increase of filament number (Fig. 4, D and E), detectable from around 20 min and completed around 40 to 50 min after addition of IAA. The thickness of actin bundles decreased concomitantly. The final situation was comparable for all three lines, but since the initial values for both filament density (lowest in L6) and bundle thickness (highest in L6) differed, the change was most pronounced in L6 compared to the moderate expressor lines L5 and L26.

Figure 3. Effect of YFP-mT on coleoptile growth and gravitropism. **A**, Mean gravitropic curvature over the YFP signal measured by western blotting and classified in relation to the strongest protein signal (observed in the line L6). The strongest group of expressors contains the lines L6, L18, L26, and L35. The graph represents data from 20 individual coleoptiles per line measured in two independent experimental series. **B**, Dose response of auxin-induced elongation over LatB in the wild type, the moderate YFP-mT expressor L5, and the strong YFP-mT overexpressor L6. Auxin-induced growth was triggered in coleoptile segments by addition of 5 μM IAA and recorded after 3 h of incubation. **C**, Dose response of elongation over IAA measured after 3 h of incubation. **D** and **E**, Dose response of gravitropic curvature over LatB in the wild type, L5, and L6 plotted as absolute mean curvature (**D**) and normalized to the mean curvature in the absence of the inhibitor (**E**). **F** and **G**, Dose response of gravitropism over auxin in the wild type, L5, and L6, plotted as absolute mean curvature (**F**) and normalized to the mean curvature in the absence of the inhibitor (**G**). Gravitropic curvature was recorded after 2 h throughout. WT, Wild type.



Auxin Stimulates Its Own Transport Depending on YFP-Talin

To assess the potential physiological effect of actin bundling in the strong expressor line L6, we measured basipetal auxin transport by application of radioactively labeled IAA to the apical ends of coleoptile segments and quantifying the radioactivity recovered in an agar block adjacent to the basal end (Fig. 5A). To get insight into the rate of transport, segment length was varied between 2.5 and 25 mm (Fig. 5B). The radioactivity recovered in the receiver decreased with increasing length of the segment and eventually reached zero for very long segments. This zero point is a measure for the distance traversed by the wave of labeled IAA during the incubation time (2 h), whereas the slope of the curve in the linear region (Fig. 5B, dotted lines) is a measure for the rate of auxin transport. In the wild type and the moderate expressor line L5, the wave of labeled IAA had moved to 25 mm (corresponding to a mean velocity of 12.5 mm h⁻¹),

and the slope was steep, whereas in the strong expressor line L6, the wave of labeled had moved to 17.5 mm (corresponding to a mean velocity of 8.5 mm h⁻¹), and the slope was shallow. The segments were preincubated in IAA to shift actin filaments from a bundled configuration into fine strands (Fig. 4) and then used for the transport assay. We recorded dose-response relations and time courses for the auxin effect on basipetal auxin transport and observed that preincubation with IAA stimulated basipetal auxin transport by about 2-fold in a dose-dependent manner. The bell-shaped dose-response curve for this stimulation peaked at around 50 μM IAA in the wild type and the moderate expressor lines L5 and L26 (Fig. 5C). The corresponding curves for the strong expressor lines L6 and L18 were similar in shape but had a peak at around 5 μM IAA, i.e. at a 10-fold lower concentration of exogenous IAA (Fig. 5E). The time course for the IAA-induced stimulation of auxin transport recorded for the optimal concentrations (50 μM for the wild type,

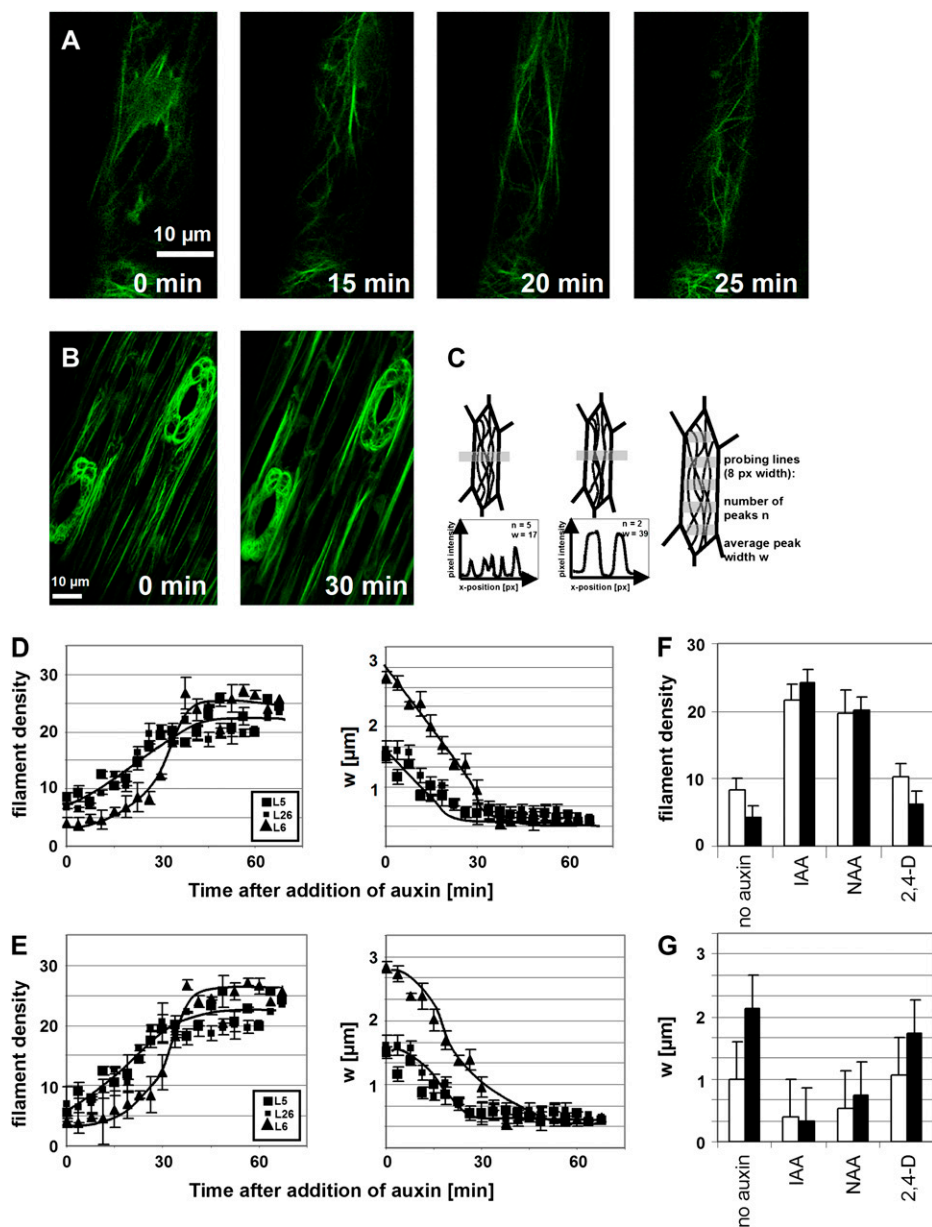
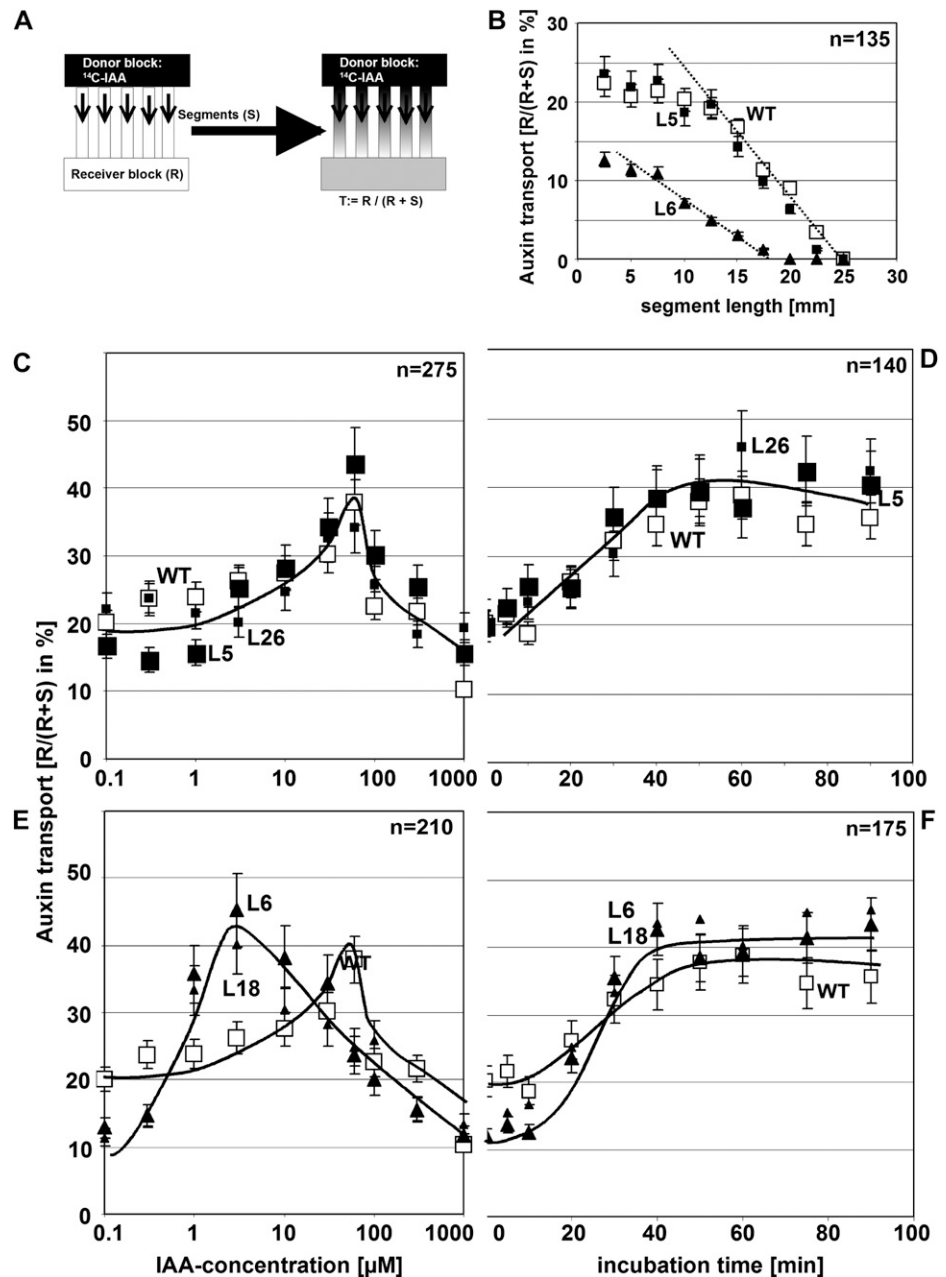


Figure 4. Effect of auxin on actin organization. A, Debundling of actin in response to 50 μM IAA added at time 0 min to coleoptiles of the strong expressor line L6. Projections of confocal stacks are shown. B, Bundling of actin after decapitation of coleoptiles of the moderate expressor line L5. Projections of z-stacks at times 0 and 30 min. C, Definition of the numerical parameters n and w to describe actin organization. n represents the mean number of actin strands over a transverse profile of defined length (i.e. the density of filaments), and w is the mean width of actin strands. Five probing lines of 8 pixel (px) width were laid over each cell to determine n and w as average over the values obtained on each probing line. D and E, Time course for the response of n (left) and w (right) to 5 μM IAA (D) and 50 μM IAA (E) in the lines L5 (moderate expression), L26 (moderate expression), and L6 (strong expression). A total of 350 individual cells were scored for each line. F and G, Response of n (F) and w (G) in the lines L5 (moderate expression; white bars) and L6 (strong expression) to different species of auxin administered for 1 h at 10 μM . Data represent the mean from 100 individual cells.

L5, and L26; 5 μM for L6 and L18, respectively) was similar, though with the stimulation becoming evident from around 20 min after addition of IAA and reaching a plateau from around 50 min after addition of IAA (Fig. 5, D and F). To test the specificity of the assay, we preincubated the coleoptiles in 5 μM NPA, an inhibitor of polar auxin transport or inverted the coleoptiles to measure apicopetal transport. In both controls, we were not able to recover significant radioactivity in the receiver blocks (Table I). To test whether actin is necessary for auxin transport, we preincubated the coleoptiles with various concentrations of LatB and cytochalasin D and observed that both compounds inhibited polar auxin transport in a dose-dependent manner (Table I) along with reducing the average density of actin filaments (see Fig. 2G for LatB). To test

for the effect of actin bundling, we depleted the tissue from endogenous auxin after coleoptile decapitating the coleoptiles and allowed the endogenous auxin to be transported out by basipetal transport. This resulted in increased bundling of actin (Fig. 4B) and a decreased basipetal transport of radioactively labeled auxin (Table I). Conversely, when actin bundling was induced by treatment with phalloidin, transport was strongly decreased in a dose-dependent manner (Table I), parallel to a reduction of actin dynamicity (Fig. 2F). In a last set of experiments, we tested whether the stimulation of basipetal transport of auxin as well as the debundling of actin could be induced by artificial auxins. We observed that 1-naphthyl acetic acid (NAA) could induce both the response of actin (Fig. 4, F and G) as well as the stimulation of basipetal

Figure 5. Effect of auxin on basipetal auxin transport. A, Quantification of polar auxin transport using ^{14}C -IAA applied through a donor block and measuring the radioactivity recovered in the receiver block as percentage of total radioactivity in segment and receiver. B, Dependence of radioactivity recovered in the receiver from segment length. C and E, Dose response of auxin transport over exogenous IAA in the wild type, L5, and L26 (moderate expression; C) compared to L6 and L18 (strong expression; E). D and F, Time course for the stimulation of auxin transport by IAA in the wild type, L5, and L26 (moderate expression; D) compared to L6 and L18 (strong expression; F). n, Numbers of coleoptiles per experiment; WT, wild type.



transport (Table I) to a degree almost comparable to that observed for IAA. In contrast, 2,4-D was almost ineffective for both the actin response (Fig. 4, F and G) and the stimulation of basipetal transport (Table I).

DISCUSSION

The directionality of auxin transport has been linked to intracellular gradients of the PIN proteins (Chen and Masson, 2006). Since the PIN proteins are continuously cycling between plasma membrane and intracellular compartments, the direction of auxin transport is expected to depend on the spatial organization of

vesicle flow. The organization of actin filaments as the central determinant of intracellular traffic should therefore control auxin fluxes through the dynamic localization of auxin-efflux carriers (Muday and Murphy, 2002; Blakeslee et al., 2005). This working hypothesis, although supported by a couple of observations (for instance, Friml et al., 2002; Sun et al., 2004) has come under dispute based on observations where the polar localization of certain members of the PIN proteins persisted the elimination of actin by inhibitors (for instance, Geldner et al., 2001; Kleine-Vehn et al., 2006; Rahman et al., 2007). Already classical work had demonstrated that a treatment with cytochalasin B that blocked cytoplasmic streaming delayed

Table 1. Effect of different pretreatments on the efficiency of auxin transport measured as mean radioactivity (with *ses*) recovered in the receiver block as a percentage of total radioactivity in receiver and segment

The pretreatments lasted for 1 h.			
Treatment Effect	Wild Type	L5	L6
Controls			
0 μM IAA (and depletion from endogenous auxin)	14.2 \pm 2.9 (<i>n</i> = 30)	12.6 \pm 1.9 (<i>n</i> = 35)	21.9 \pm 2.7 (<i>n</i> = 39)
10 μM IAA	28.0 \pm 3.4 (<i>n</i> = 35)	26.8 \pm 2.9 (<i>n</i> = 40)	35.2 \pm 3.0 (<i>n</i> = 38)
10 μM IAA, inverted	4.8 \pm 1.4 (<i>n</i> = 30)	6.8 \pm 2.2 (<i>n</i> = 33)	5.2 \pm 2.0 (<i>n</i> = 28)
5 μM NPA	2.0 \pm 0.4 (<i>n</i> = 20)	0.8 \pm 0.5 (<i>n</i> = 25)	3.2 \pm 1.0 (<i>n</i> = 29)
LatB			
10 μM IAA + 1 μM LatB	26.4 \pm 3.0 (<i>n</i> = 32)	27.5 \pm 3.1 (<i>n</i> = 42)	33.3 \pm 2.5 (<i>n</i> = 40)
10 μM IAA + 10 μM LatB	14.7 \pm 2.1 (<i>n</i> = 39)	17.5 \pm 2.0 (<i>n</i> = 35)	29.2 \pm 3.5 (<i>n</i> = 38)
10 μM IAA + 100 μM LatB	12.2 \pm 1.4 (<i>n</i> = 35)	13.6 \pm 1.7 (<i>n</i> = 33)	26.5 \pm 2.8 (<i>n</i> = 40)
Cytochalasin D (CytD)			
10 μM IAA + 1 μM CytD	25.0 \pm 2.9 (<i>n</i> = 30)	26.1 \pm 2.5 (<i>n</i> = 35)	30.2 \pm 1.9 (<i>n</i> = 30)
10 μM IAA + 10 μM CytD	13.1 \pm 2.8 (<i>n</i> = 28)	14.1 \pm 2.6 (<i>n</i> = 35)	27.9 \pm 2.7 (<i>n</i> = 35)
Phalloidin (Pha)			
10 μM IAA + 1 μM Pha	21.2 \pm 1.9 (<i>n</i> = 24)	16.4 \pm 1.5 (<i>n</i> = 25)	33.5 \pm 2.4 (<i>n</i> = 29)
10 μM IAA + 10 μM Pha	8.9 \pm 2.1 (<i>n</i> = 27)	10.7 \pm 2.8 (<i>n</i> = 19)	28.4 \pm 2.7 (<i>n</i> = 32)
Artificial auxins			
Decapitation + 0 μM IAA	14.2 \pm 2.9 (<i>n</i> = 30)	12.6 \pm 1.9 (<i>n</i> = 35)	21.9 \pm 2.7 (<i>n</i> = 39)
10 μM NAA	24.5 \pm 2.1 (<i>n</i> = 35)	22.2 \pm 1.9 (<i>n</i> = 41)	30.7 \pm 2.8 (<i>n</i> = 35)
10 μM 2,4-D	14.5 \pm 1.1 (<i>n</i> = 33)	11.7 \pm 1.5 (<i>n</i> = 38)	17.7 \pm 2.3 (<i>n</i> = 30)

the entry of labeled auxin into the transport stream (most pronounced in oat coleoptiles and less in corn [*Zea mays*]), but did not alter the rate of auxin transport (Cande et al., 1973).

On the other hand, treatment with the actin-stabilizing compound jasplakinolide inhibited auxin efflux in *Arabidopsis* suspension cultures, and the phytohormones TIBA and 2-(1-pyrenoyl) benzoic acid were found to bundle actin in root cells as well as in nonplant cells, indicating that they exert their effect on auxin flow by interacting with actomyosin (Dhonukshe et al., 2008). Interestingly, the phytohormone action of TIBA along with *N*-ethylmaleimide was originally discovered as most potent inhibitors in experiments targeted to the role of SH-rich proteins for auxin transport (Leopold, 1961). Both compounds have been classically used as inhibitors of sulfhydryl groups, and *N*-ethylmaleimide was widely used as an efficient blocker of actomyosin activity, for instance, in the context of cytoplasmic streaming (Nagai and Rebhun, 1966). Thus, the study by Dhonukshe et al. (2008) confirms classical work suggesting that TIBA primarily affects actomyosin and inhibits auxin transport only secondarily. In contrast, NPA was not found to alter actin organization in nonplant cells, although it does so in *Arabidopsis* roots (Rahman et al., 2007; Dhonukshe et al., 2008). This suggests that NPA primarily affects auxin transport and, secondarily through the response of actin to auxin, the organization of microfilaments. The controversy on this issue may also be caused by the fact that actin is not only participating in the endocytotic pathway but also affects anterograde transport. The sensitivity of these actin functions to the different inhibitors will depend on the respective dynamicity of these

functionally different actin structures that are unlikely to be constant but are regulated, such that the outcome of a given inhibitor experiment will strongly depend on the physiological state of the investigated organ or cell type.

To clarify this issue, we decided to test the relationship between actin organization and auxin transport in a system, where both parameters are amenable to observation and manipulation. We therefore returned to the classical system for the physiology of auxin transport, the Graminean coleoptile (for a classical review, see Goldsmith, 1977). To manipulate actin organization, we used a genetic approach, where we expressed the actin-binding protein mouse talin in fusion with YFP. Mouse talin has been proposed to compete with endogenous actin depolymerization factors for binding sites on actin in transgenic *Arabidopsis* (Ketelaar et al., 2004) leading to a reduction of monomer turnover such that the actin filaments are progressively trapped in a bundled configuration. By using different, independent transgenic lines, we were able to obtain variable degrees of actin bundling depending on the expression level of mouse talin. Whereas a moderate expression of talin left the configuration and dynamics of actin basically untouched, we observed bundling of actin filaments in lines that overexpressed talin strongly. In these strong expressor lines, the characteristic alterations of actin organization and dynamics were accompanied by alterations of actin-dependent growth responses, such as gravitropic bending or auxin-induced cell elongation (Fig. 6). Moreover, the sensitivity of these physiological responses to LatB (a drug that sequesters monomeric actin and thus eliminates actin filaments due to their

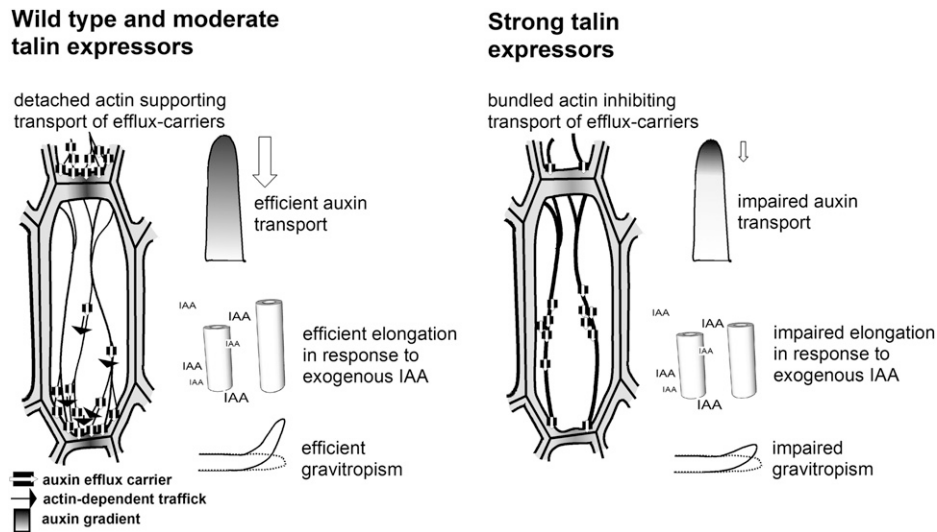


Figure 6. Model for the functional effects of talin overexpression in rice. Fine actin filaments in wild type and moderate talin expressors support the polar localization of auxin efflux carriers and thus efficient auxin transport. Due to the role of actin in cell elongation, they also support efficient elongation of coleoptile segments in response to exogenous IAA. Both actin functions (auxin transport and cell elongation) contribute to the efficient gravitropism of rice coleoptiles. In strong talin expressors, excessive actin bundling impairs the polar localization of auxin efflux carriers and, thus, auxin transport. In addition, the elongation response to exogenous IAA is reduced. Both effects lead to a reduced gravitropic response.

innate turnover) was reduced in the strong expressor lines. Bundled actin has been repeatedly observed to be accompanied by a reduced physiological response to auxins in a couple of different systems (delayed auxin transport in corn coleoptiles after treatment with cytochalasin B [Cande et al., 1973], auxin sensitivity of cell elongation in coleoptiles of corn or rice [Wang and Nick, 1998; Waller et al., 2002], and auxin-dependent synchrony of cell division in tobacco cells [Maisch and Nick, 2007]).

On the other hand, classical work using cytochalasin B reported that the rate of auxin transport was not affected, although cytoplasmic streaming was inhibited and actin filaments appeared to be bundled (Cande et al., 1973). There was, however, a clear delay in the entrance of labeled IAA into the transport stream. In contrast to these observations, we observe not only that the wave of labeled IAA moves slower in the strong expressor line L6 (8.5 mm h^{-1} compared to 12.5 mm h^{-1} in the wild type and the moderate expressor line L5) but also that the slope of transport is reduced in the line where actin is bundled.

Our observations link the amplitude of talin overexpression with the physiological effect of actin bundling. When actin bundling was induced in the wild type by phalloidin (mimicking the situation in the overexpressor line), this reduced actin dynamicity and auxin transport. These correlations demonstrate that a debundled configuration of actin is necessary for efficient responses to auxin, including elongation growth, gravitropic bending, and polar transport of auxin.

By addition of exogenous IAA, we were able to restore a relatively debundled actin configuration in

the strong talin expressors. This rescue was accompanied by a stimulation of longitudinal auxin transport equivalent to the maximal amplitudes observed in the wild type upon optimal concentrations of auxin. Moreover, gravitropic curvature as physiological response dependent on polar auxin transport was recovered as well, again to levels that were only 15 degrees lower than those reached in the wild type.

A closer look reveals that the dose-response curve for the stimulation of auxin transport peaked at concentrations of IAA for the wild type and moderate expressing line (Fig. 5C) that inhibited gravitropic curvature in those lines (Fig. 3F). This apparent discrepancy can be explained by the fact that gravitropism depends on the growth differential between the two flanks of the stimulated organ. The optimal concentration for the stimulation of elongation in rice coleoptiles is at $5 \mu\text{M}$ IAA (Fig. 3C; Wang and Nick, 1998). At $50 \mu\text{M}$, elongation is beyond the peak of the bell-shaped dose-response curve such that gravitropic curvature is strongly impaired.

Interestingly, the strong YFP-talin overexpressor is more sensitive to the stimulating effects of IAA on polar auxin transport (Fig. 5D). This might be caused by a higher pool of actin present in those lines (Fig. 1, F and G) that upon debundling triggered by auxin becomes available for the transport of auxin-efflux carriers. Consistently, the strong overexpressors produce more actin filaments when pretreated with exogenous IAA (Fig. 4D). Thus, the phenotype of the strong talin expressors can be completely rescued by debundling of actin in response to exogenous IAA. Therefore, in these lines, a debundled config-

uration of actin is sufficient for efficient responses to auxin.

The debundling of actin in response to IAA was found to become manifest from 20 min and to reach a plateau around 60 min after addition of IAA, parallel to the time course for the stimulation of auxin transport by exogenous IAA. The debundling response and the stimulation of auxin transport can be triggered by NAA, whereas 2,4-D is almost ineffective. Thus, the activity pattern of the three auxins for debundling of actin and stimulation of actin are strictly parallel as well as the time course of the two auxin responses. In summary, the debundling of actin induced by auxins and the stimulation of auxin transport by auxins are similar in their specific quality.

Therefore, actin debundling is both necessary and sufficient for auxin-induced stimulation of auxin transport, it follows the same time course, and it can be triggered by IAA and NAA, but not by 2,4-D. The most straightforward model to explain these findings is a causal relationship between auxin-induced debundling of actin and auxin-induced stimulation of auxin transport. By inducing a dissociation of actin bundles into finer strands, auxin might release auxin-efflux carriers, such as the PIN proteins from sequestration in intracellular compartments such that these carriers can be delivered to their site of action at the plasma membrane. However, since endocytosis is actin dependent as well, it is not trivial to pinpoint its cellular function experimentally. For instance, when actin bundling was induced by TIBA in BY-2 cells, this produced an increase of PIN1-GFP in the cytoplasm within 30 min but still left a strong signal at the plasma membrane (Dhonukshe et al., 2008). There will be no clear outcome of this type of experiment without kinetic and quantitative approaches. On the other hand, consistent with the actin sequestration model, auxin has been observed to promote the localization of cycling PIN proteins at the plasma membrane (Paciorek et al., 2005).

It should be mentioned in this context that, in *Arabidopsis* roots, IAA induced a bundling of actin filaments. This, at first sight, appears to be a discrepancy. However, the auxin sensitivity in roots is much higher than that of shoots, such that an increase of auxin will cause an inhibition of growth (because the endogenous auxin content is already beyond the peak of the bell-shaped dose-response relation for auxin-induced growth). In shoots and coleoptiles, auxin sensitivity is much lower, such that the endogenous auxin content will only produce half-maximal growth, and addition of exogenous auxin will therefore stimulate growth. However, when the exogenous concentration of auxin rises beyond the optimum of the bell-shaped auxin dose-response curve, this causes an inhibition of growth and a bundling of actin (Waller et al., 2002), similar to the situation observed in roots (Rahman et al., 2007). A part of the controversy about the role of actin in polar auxin transport might be caused by the fact that it is not easy (and possibly in some cases not feasible) to

compare data that have been collected in different tissues or species.

The implications of this model are to be explored, but already at this stage it can be used to derive characteristic properties of basipetal auxin transport. For instance, the model predicts that the transport of IAA should oscillate because auxin will, through reorganization of actin, stimulate auxin efflux such that the intracellular level of auxin will drop, which in turn will result in a bundled configuration of actin, such that auxin-efflux carriers will be sequestered culminating in a reduced efflux such that auxin received from the adjacent cells will accumulate and trigger a new cycle. The frequency of these oscillations should depend on the dynamics of actin reorganization (around 20 min) and the speed of PIN cycling (in the range of 5–10 min) and is expected to be in the range of 25 to 30 min. In fact, classical experiments on basipetal auxin transport in coleoptiles report such oscillations with a period of 25 min (Hertel and Flory, 1968).

We therefore arrive at a model of a self-referring regulatory circuit between polar auxin transport and actin organization where auxin promotes its own transport by shaping actin filaments. This circuit seems to act in concert with other mechanisms of positive feedback, such as auxin-dependent expression of auxin-efflux carriers, such as PIN (Peer et al., 2004; Vieten et al., 2005) or P-glycoprotein (for a recent review, see Titapiwatanakun and Murphy, 2009), which might contribute to the self-amplification of auxin transport that is a central element in current models of auxin-dependent patterning.

MATERIALS AND METHODS

Generation and Characterization of the Rice YFP-Talin Lines

The p35S-YFP-mT construct (Brandizzi et al., 2002) in the binary vector (pVKH18En6) was a kind gift of Dr. Federica Brandizzi (Oxford Brookes University, UK) and was introduced to rice (*Oryza sativa*) calli via *Agrobacterium tumefaciens*-mediated transformation (Hiei et al., 1997; Lee et al., 1999). Briefly, scutellum-derived calli were generated on 2 N₆ medium from mature seeds of *O. sativa* subsp. *japonica* 'Dongjin'. The calli were cocultured with *Agrobacterium* for 3 d, and transformants were selected on 2 N₆ medium containing 1 mg L⁻¹ 2,4-D, 0.5 mg L⁻¹ benzyl-adenine purine, and 40 mg L⁻¹ hygromycin in darkness. Shoots were regenerated on shoot induction medium containing 0.1 mg L⁻¹ NAA and 1 mg L⁻¹ kinetin under continuous light. The transgenic rice plants were raised to maturity in a greenhouse. Thirty-eight independent transformants could be recovered and were self-pollinated. Seeds from those lines were raised to the five-leaf state and tested for the presence of the transgene by genomic PCR using primers 5'-TTAGTGCTCGTCTCGAAGCTCTG-3' and 5'-CAAATCCTAGAAGCTGCCAAGTCC-3' against the YFP-mT insert (Brandizzi et al., 2002). Homozygous plants were identified, raised to maturity, and self-pollinated, and seeds were obtained. The expression of the fusion protein was tested in three independent experimental series, first qualitatively by fluorescence microscopy (see below) and then quantitatively by western analysis of total proteins extracted from etiolated coleoptiles raised for 6 d at 25°C using antibodies against the FP-tag (polyclonal rabbit-anti-FP Nr. 8367-2; BD Biosciences). The relative abundance of the talin-YFP fusion protein in these total extracts was quantified as described by Waller et al. (2002) and calculated as proportion to the abundance in the strongest expressor, line 6, that was loaded as internal standard onto each gel.

Microscopy

To test whether the YFP-mT decorated actin filaments ubiquitously, actin filaments were visualized by TexasRed-phalloidin (Molecular Probes) in epidermal cells of etiolated coleoptiles as described by Waller and Nick (1997) and viewed by confocal laser scanning microscopy (TCS SP1; Leica) using a dual-wavelength (ArKr laser lines 488 and 564 nm) configuration. To monitor actin dynamics *in vivo*, intact coleoptiles were mounted and observed on slides under green safelight as described by Himmelspach et al. (1999), and the epidermis was observed over time using the fixed-stage configuration of the confocal laser scanning microscope with the 488-nm laser line of the ArKr laser and a four-frame averaging protocol.

Measurement of Actin Dynamics and Bundling

The bundling of actin filaments was quantified according to Schwarzerová et al. (2002) using the integrated density tool of the Image J software (National Institute of Health) on projections of z-stacks recorded over the epidermal cell layer. The width of the probing line was set to eight pixels to integrate over local differences of fluorescence intensity, and a grid of five lines was recorded and averaged for each cell as depicted in Figure 3C. From these profiles of fluorescence intensity, the average thickness of actin bundles as well as the average frequency of bundles (as number of bundles per 10 μm of the probing line) were determined as described by Schwarzerová et al. (2002). Twenty individual cells from five individuals were scored for each time point of the time courses shown in Figure 4, D and E. To quantify dislocations of actin filaments over time as a measure for actin dynamics, time series were recorded for individual focal planes and the absolute differentials were constructed for the images of subsequent time points t_1 and t_2 by subjecting each individual pixel p_i to the operation $|p_{i,t_2} - p_{i,t_1}|$ as depicted in Figure 2C. Frequency histograms over pixel intensities were constructed over these differentials using the histogram tool of Photoshop (Adobe) as shown exemplarily in Figure 2D. Filaments that absolutely keep their position over time would yield a differential of 0, whereas filaments that shift either in the xy-plane or in the z-direction (thus disappearing from the confocal image) would contribute with $2 \sum p_i$ with p_i representing the intensity of the individual pixels that constitute the image of the respective filament. The corresponding histograms over intensity of this differential would therefore be shifted toward higher values in a situation where actin filaments change dynamically. Thus, the median of these histograms is a measure for overall displacements of the filaments. For each transgenic line, time courses of 53 individual epidermal cells from 5 to 10 individual plants were recorded and averaged as shown in Figure 2, D to F.

Measurement of Gravitropism and Auxin-Dependent Growth

Five rice seeds were fixed, embryo up, with medical glue (B401; Factor II), 5 mm below the edge of a microscopy slide. The slides were placed in conventional staining trays in Plexiglas boxes (95 \times 95 \times 60 mm). The Plexiglas boxes were filled with deionized water so that the seeds were only partially covered to ensure optimal oxygen access and germination. After 5 d of cultivation in the dark at 25°C, the seedlings were used for the assays on gravitropism and growth. Gravitropic curvature was measured 2 h after the onset of a continuous stimulus of 1 g (inclination by 90°) as described by Gutjahr and Nick (2006). All manipulations of seedlings were performed under green safelight (λ_{max} 550 nm). For dose-response curves, seedlings were preincubated vertically for 1 h in various concentrations of actin inhibitors (LatB and cytochalasin D), inhibitors of polar auxin transport (NPA and TIBA), or auxins (IAA, NAA, and 2,4-D) in 5 mM MES buffer, pH 7.0, and then tilted by 90°. For the growth assays, coleoptile segments with a length of 10 mm were excised 3 to 13 mm below the tip and incubated under continuous rotation on a topover shaker in complete darkness for 5 h in the presence of variable concentrations of LatB and 5 μM IAA, the auxin concentration optimal for segment elongation (Wang and Nick, 1998) in 5 mM MES buffer, pH 7.0. Length increments after 5 h were determined under a stereomicroscope.

Measurement of Longitudinal IAA Transport

Longitudinal IAA transport was measured according to Gutjahr and Nick (2006) with minor modifications. Five vertically oriented coleoptile segments were preincubated for 1 h in variable concentrations of IAA (or alternatively in

inhibitors or other auxins as shown in Table I) and then sandwiched between two agar blocks (8 \times 2 \times 1 mm, 1.5% agar). If not stated otherwise, segment length was 10 mm. Care was taken that the entire surface of the cuts was in contact with the agar block and that the segments did not touch each other laterally to avoid bypasses of IAA. The donor block at the apical surface contained 0.1 μM IAA and 0.1 μCi (1 Ci = 37 GBq) of [¹⁴C]IAA (American Radiolabeled Chemicals) but no drugs. After incubation for 2 h in a moist chamber at 25°C, the contact face of the segment with the donor was trimmed by 1 mm to remove potential contamination of the tissue by radioactive agar from the donor block. Then, donor blocks, receiver blocks, and segments were collected separately in 5 mL of Rotizint scintillation fluid (Roth) with 500 μL of 5 mM Tris buffer and moderately shaken overnight at 25°C for equilibration. Radioactivity in counts per min was determined by scintillation counting (LS 5000CE; Beckmann). Basal values were determined with nonradioactive segments and plain agar blocks, respectively. Transport was calculated as $100 \times [R/(R + S)]$, with R radioactivity recovered in the receiver block corrected for the basal value for receiver blocks and S radioactivity in the segment corrected for the basal value for segments. Inverted segments were used as a negative control for basipetal transport.

ACKNOWLEDGMENTS

We thank Dr. Federica Brandizzi (Oxford Brookes University, UK) for the p35S-YFP-mT construct, Angelika Piernitzki (Botanical Garden of the University of Karlsruhe) for the propagation of the YFP-mTalin lines, Dr. Michael Riemann (Botanical Institute 1, University of Karlsruhe) for help with the genotyping of the lines, and Dr. Manfred Focke (Botanical Institute 2, University of Karlsruhe) for access to the scintillation counter.

Received April 22, 2009; accepted July 17, 2009; published July 24, 2009.

LITERATURE CITED

- Berleth T, Sachs T (2001) Plant morphogenesis: long-distance coordination and local patterning. *Curr Opin Plant Biol* 4: 57–62
- Blakeslee JJ, Peer WA, Murphy AS (2005) Auxin transport. *Curr Opin Plant Biol* 8: 494–500
- Brandizzi F, Snapp EL, Roberts AG, Lippincott-Schwartz J, Hawes C (2002) Membrane protein transport between the endoplasmic reticulum and the Golgi in tobacco leaves is energy dependent but cytoskeleton independent: evidence from selective photobleaching. *Plant Cell* 14: 1293–1309
- Butler JH, Hu S, Brady SR, Dixon MW, Muday GK (1998) *In vitro* and *in vivo* evidence for actin association of the naphthylphthalamic acid-binding protein from zucchini hypocotyls. *Plant J* 13: 291–301
- Cande WZ, Goldsmith MHM, Ray PM (1973) Polar auxin transport and auxin-induced elongation in the absence of cytoplasmic streaming. *Planta* 111: 279–296
- Chen R, Masson PH (2006) Auxin transport and recycling of PIN proteins in plants. In J Šamaj, F Baluška, D Menzel, eds, *Plant Endocytosis*. Springer, Berlin, pp 139–157
- Coué M, Brenner SL, Spector I, Korn ED (1987) Inhibition of actin polymerization by latrunculin A. *FEBS Lett* 213: 316–318
- Dhonukshe P, Grigoriev I, Fischer R, Tominaga M, Robinson DG, Hašek J, Paciorek T, Petrášek J, Seifertová D, Tejos R, et al (2008) Auxin transport inhibitors impair vesicle motility and actin cytoskeleton dynamics in diverse eukaryotes. *Proc Natl Acad Sci USA* 105: 4489–4494
- Friml J, Wišniowska J, Benková E, Mendgen K, Palme K (2002) Lateral relocation of auxin efflux regulator PIN3 mediates tropism in Arabidopsis. *Nature* 415: 806–809
- Geldner N, Anders N, Wolters H, Keicher J, Kornberger W, Müller P, Delbarre A, Ueda T, Nakano A, Jürgens G (2003) The Arabidopsis GNOM ARF-GEF mediates endosomal recycling, auxin transport, and auxin-dependent plant growth. *Cell* 112: 219–230
- Geldner N, Friml J, Stierhof YD, Jürgens G, Palme K (2001) Auxin transport inhibitors block PIN1 cycling and vesicle trafficking. *Nature* 413: 425–428
- Goldsmith MHM (1977) The polar transport of auxin. *Annu Rev Plant Physiol* 28: 439–478
- Gutjahr C, Nick P (2006) Acrylamide inhibits gravitropism and destroys microtubules in rice coleoptiles. *Protoplasma* 227: 211–222

- Hertel R, Flory R (1968) Auxin movement in corn coleoptiles. *Planta* **82**: 123–144
- Hiei Y, Komari T, Kubo T (1997) Transformation of rice mediated by *Agrobacterium tumefaciens*. *Plant Mol Biol* **35**: 205–218
- Himmelspach R, Wymer CL, Lloyd CW, Nick P (1999) Gravity-induced reorientation of cortical microtubules observed *in vivo*. *Plant J* **18**: 449–453
- Holweg C (2007) Living markers for actin block myosin-dependent motility of plant organelles and auxin. *Cell Motil Cytoskeleton* **64**: 69–81
- Holweg C, Süßlin C, Nick P (2004) Capturing *in-vivo* dynamics of the actin cytoskeleton. *Plant Cell Physiol* **45**: 855–863
- Ketelaar T, Anthony RG, Hussey PJ (2004) Green fluorescent protein-mTalin causes defects in actin organization and cell expansion in *Arabidopsis* and inhibits actin depolymerizing factor's actin depolymerizing activity *in vitro*. *Plant Physiol* **136**: 3990–3998
- Kleine-Vehn J, Dhonukshe P, Swarup R, Bennett M, Friml J (2006) Subcellular trafficking of the *Arabidopsis* auxin influx carrier AUX1 uses a novel pathway distinct from PIN1. *Plant Cell* **18**: 3171–3181
- Lee S, Jeon JS, Jung KH, An G (1999) Binary vectors for efficient transformation of rice. *J Plant Biol* **42**: 310–316
- Leopold AC (1961) The transport of auxin. In W Ruhland, ed, *Encyclopedia of Plant Physiology*, Vol 14. Springer, Berlin, pp 671–682
- Lomax TL, Muday GK, Rubery PH (1995) Auxin transport. In P Davies, ed, *Plant Hormones: Physiology, Biochemistry, and Molecular Biology*. Kluwer, Dordrecht, The Netherlands, pp 509–530
- Maisch J, Nick P (2007) Actin is involved in auxin-dependent patterning. *Plant Physiol* **143**: 1695–1704
- Merks RMH, Van de Peer Y, Inzé D, Beeemster GTS (2007) Canalization without flux sensors: a traveling-wave hypothesis. *Trends Plant Sci* **12**: 1360–1385
- Muday GK, Murphy AS (2002) An emerging model of auxin transport regulation. *Plant Cell* **14**: 293–299
- Nagai R, Rebhun LI (1966) Cytoplasmic microfilaments in streaming *Nitella* cells. *J Ultrastruct Res* **14**: 571–589
- Paciorek T, Zažimalová E, Ruthardt N, Petrášek J, Stierhof YD, Kleine-Vehn J, Morris DA, Emans N, Jürgens G, Geldner N, et al (2005) Auxin inhibits endocytosis and promotes its own efflux from cells. *Nature* **435**: 1251–1256
- Peer WA, Bandyopadhyay A, Blakeslee JJ, Makam SN, Chen RJ, Masson PH, Murphy AS (2004) Variation in expression and protein localization of the PIN family of auxin efflux facilitator proteins in flavonoid mutants with altered auxin transport in *Arabidopsis thaliana*. *Plant Cell* **16**: 1898–1911
- Petrášek J, Mravec J, Bouchard R, Blakeslee JJ, Abas M, Seifertová D, Wisniewska J, Tadele Z, Kubes M, Covanová M, et al (2006) PIN proteins perform a rate-limiting function in cellular auxin efflux. *Science* **312**: 914–918
- Rahman A, Bannigan A, Sulaman W, Pechter P, Blancaflor EB, Baskin TI (2007) Auxin, actin and growth of the *Arabidopsis thaliana* primary root. *Plant J* **50**: 514–528
- Reinhard D, Mandel T, Kuhlemeier C (2000) Auxin regulates the initiation and radial position of plant lateral organs. *Plant Cell* **12**: 507–518
- Rubery PH (1990) Phytotropins: receptors and endogenous ligands. In J Roberts, C Kirk, M Venis, eds, *Hormone Perception and Signal Transduction in Animals and Plants*. The Company of Biologists Ltd., Cambridge, UK, pp 119–145
- Sachs T (1969) Polarity and the induction of organized vascular tissues. *Ann Bot (Lond)* **33**: 263–275
- Sachs T (2000) Integrating cellular and organismic aspects of vascular differentiation. *Plant Cell Physiol* **41**: 649–656
- Schwarzerová K, Zelenková S, Nick P, Opatrný Z (2002) Aluminum-induced rapid changes in the microtubular cytoskeleton of tobacco cell lines. *Plant Cell Physiol* **43**: 207–216
- Sun H, Basu S, Brady SR, Luciano RL, Muday GK (2004) Interactions between auxin transport and actin cytoskeleton in developmental polarity of *Fucus distichus* embryos in response to light and gravity. *Plant Physiol* **135**: 266–278
- Sweeney BM, Thimann KV (1937) The effect of auxins on protoplasmic streaming. *J Gen Physiol* **21**: 439–461
- Titapiwatanakun B, Murphy AS (2009) Post-transcriptional regulation of auxin transport proteins: cellular trafficking, protein phosphorylation, protein maturation, ubiquitination, and membrane composition. *J Exp Bot* **60**: 1093–1107
- Vieten A, Vanneste S, Wiśniewska J, Benková E, Benjamins R, Beeckman T, Luschnig C, Friml J (2005) Functional redundancy of PIN proteins is accompanied by auxin dependent cross-regulation of PIN expression. *Development* **132**: 4521–4531
- Waller E, Nick P (1997) Response of actin microfilaments during phytochrome-controlled growth of maize seedlings. *Protoplasma* **200**: 154–162
- Waller E, Riemann M, Nick P (2002) A role for actin-driven secretion in auxin-induced growth. *Protoplasma* **219**: 72–81
- Wang QY, Nick P (1998) The auxin response of actin is altered in the rice mutant *Yin-Yang*. *Protoplasma* **204**: 22–33